Azobenzene photoswitches in bulk materials

Marcus Böckmann, Nikos L. Doltsinis,* and Dominik Marx
Lehrstuhl für Theoretische Chemie, Ruhr-Universität Bochum, 44780 Bochum, Germany
(Received 26 October 2007; revised manuscript received 4 June 2008; published 2 September 2008)

A nonadiabatic two-scale quantum-classical dynamics method is developed to allow for dynamical simulation of photoinduced processes and reactions in chemically complex condensed-matter systems such as photosensitive liquid crystals. A first application to photoswitching of azobenzene in the bulk reveals not only valuable insights into the excited-state dynamics underlying the *cis* to *trans* transformation, but also into the influence of the condensed phase environment on mechanism and relaxation time scales compared to vacuum.

DOI: 10.1103/PhysRevE.78.036101 PACS number(s): 82.20.Gk, 37.10.Vz, 71.15.Pd, 82.30.Qt

The possibility to reversibly switch between the *cis* and *trans* forms of azobenzene (AB) by exposing it to light of a suitable wavelength has made AB the most widely used photoswitch in physics, (bio)chemistry, and materials science [1–12]. Optomechanical applications exploit the fact that in going from *cis* to *trans*, the AB molecule substantially expands (by ≈2.4 Å; see Fig. 1). AB has, for instance, been built into synthetic peptides and foldamers to photocontrol their conformational dynamics [4,8,12]. Attempts to design molecular nanomachines and optomechanical cycles that convert light into mechanical action have been based on the same principle [10,11]. In materials science, AB functional units are incorporated in polymers and liquid crystals to manipulate reversibly their shape or phase order by irradiation [7,9], properties that may be exploited, e.g., in photoaddressable image storage media [6]. Finally, photochromic molecules such as AB can also be used as optoelectronic building blocks in molecular electronics due to their photoswitchable, isomer-dependent conductivity [13,14].

Despite the widespread use of AB-based photoswitches in practical applications, the details of the underlying photoisomerization process had been poorly understood for decades. Only a recent surge of *ab initio* quantum-chemical studies has finally established a consensus on the basic photoswitching mechanism *of isolated AB molecules in the gas phase* [15–21]. It is now believed that photoexcitation to the S_1 $(n \rightarrow \pi^*)$ excited state results in out-of-plane torsional isomerization. While understanding photoisomerization in a single AB molecule is certainly a necessary and important step, all applications such as the aforementioned ones occur in condensed phases thus involving coupling of the AB chromophore to complex fluctuating environments.

Computational studies of photoswitching in complex condensed matter are far beyond the capabilities of current *ab initio* methods due to their computational demand. A viable option is the use of quantum-classical ("QM/MM") two-scale techniques [22] in which the photoactive chromophore is treated using a quantum-mechanical (QM) electronic structure method, whereas the photoinactive environment is approximated by classical force fields, i.e., molecular mechanics (MM). Here we present a powerful and versatile nonadiabatic QM/MM (na-QM/MM) simulation method that involves not only the excited state as such but includes a proper nonadiabatic coupling to the ground state in a fully dynamical framework. In a nutshell, the QM subsystem is treated within density-functional theory [23,24], where nonadiabatic effects are included in a mixed quantum-classical manner through Tully's surface hopping algorithm [25]. This approach transcends the Born-Oppenheimer approximation and thus allows one to investigate the real-time dynamics of complex photoinduced processes, including excited-state chemical reactions and radiationless decay, in molecular condensed matter.

This na-QM/MM method is applied here to photoisomerization in bulk liquid AB, which is a prototype of photoswitchable condensed-matter systems [1,2,26]. In particular, the study gives important insights into the effects of molecular environments and confinement on the photoisomerization mechanism, which provides valuable clues to understand photoaddressable polymeric or liquid-crystalline materials used in actual applications [1–12].

Inclusion of nonadiabatic effects into otherwise classical nuclear dynamics is achieved using a mixed quantum-classical approach [25] in which the nuclei follow a single classical trajectory, $\mathbf{R}(t)$, whereas the electrons in the QM subsystem are described by $\Phi^{\mathrm{QM/MM}}$ satisfying the time-dependent Schrödinger equation (TDSE). The QM/MM coupling is established via a Hamiltonian [27] $\mathcal{H}^{\mathrm{QM/MM}}$, which is a function of *all* the nuclear coordinates, i.e., both the QM and the MM subsystems. Likewise, the total wave function, $\Phi^{\mathrm{QM/MM}}$, depends on the entire set of nuclear coordinates and is expanded,

$$\Phi^{\mathrm{QM/MM}}(\mathbf{r},\mathbf{R},t) = \sum_i a_i(t)\,\phi_i^{\mathrm{QM/MM}}(\mathbf{r},\mathbf{R}), \tag{1}$$

in terms of known functions, $\phi_i^{\mathrm{QM/MM}}(\mathbf{r},\mathbf{R})$. The time-dependent expansion coefficients, $a_i(t)$, are determined by inserting this ansatz into the TDSE, resulting in a system of coupled differential equations,

$$\dot{a}_i(t) = -\frac{i}{\hbar} a_i(t) E_i^{\mathrm{QM/MM}} - \sum_j a_j(t) C_{ij}^{\mathrm{QM/MM}}, \tag{2}$$

where $E_i^{\mathrm{QM/MM}}$ is the energy of electronic state i, and $C_{ij}^{\mathrm{QM/MM}} = \langle \phi_i^{\mathrm{QM/MM}} | \partial/\partial t | \phi_j^{\mathrm{QM/MM}} \rangle$ are the nonadiabatic couplings between states i and j.

*Author to whom correspondence should be addressed. Present address: Department of Physics, King's College London, London WC2R 2LS, United Kingdom, nikos.doltsinis@kcl.ac.uk

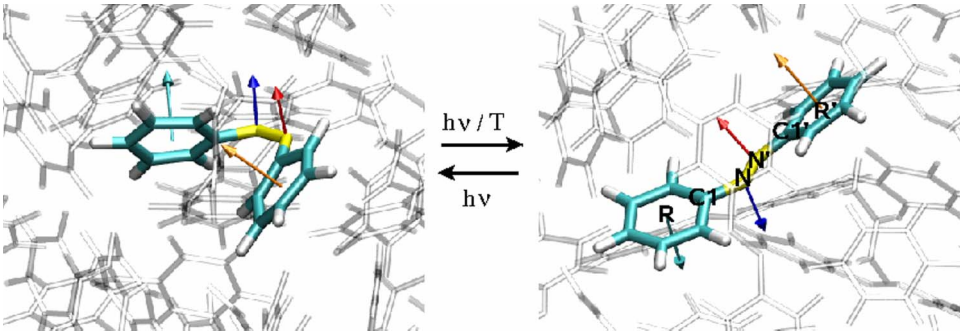

FIG. 1. (Color online) Representative snapshots of *cis* (left) and *trans* (right) conformations of AB from na-QM/MM simulations with normal vectors of the aromatic rings [$\mathbf{n}^{\mathrm{R}}$, cyan (light gray); $\mathbf{n}^{\mathrm{R}'}$, orange (light gray)] and of the $\mathrm{C}^{(1)}\mathrm{NN}'$ and $\mathrm{NN}'\mathrm{C}^{(1')}$ coordination planes [$\mathbf{n}^{\mathrm{N}}$, blue (dark gray); $\mathbf{n}^{\mathrm{N}'}$, red (medium gray)]. In the central na-QM AB molecule, the azo group –N=N'– is yellow (light gray), C and H are cyan (light gray) and white, whereas the MM AB molecules of the liquid environment are transparent.

The present two-state implementation couples nonadiabatically the closed-shell Kohn-Sham ground state, $\phi_0^{\mathrm{QM/MM}}$, to the reorthonormalized restricted open-shell Kohn-Sham (ROKS) representation [28,29] of the S_1 excited state, $\phi_1^{\mathrm{QM/MM}}$, following the successful single-scale na-QM technique [23,30,31]. As a two-determinant representation (for reviews, see Refs. [24,32]), the ROKS S_1 state provides an improved reference to compute nonadiabatic couplings [33], and yields reliable S_1 nonradiative lifetimes and decay mechanisms when nonadiabatically coupled to the KS ground state [23,30,31]. In addition to this QM component, a force-field parametrization suitable for condensed phase simulations [26] must be used to define the MM part of $\mathcal{H}^{\mathrm{QM/MM}}$. Importantly, the consistent electron density in the excited state, which deviates from that of the ground state, has to be used to include the QM↔MM electrostatic coupling within $\mathcal{H}^{\mathrm{QM/MM}}$.

The na-QM/MM simulation method has been implemented in the *ab initio* molecular-dynamics package CPMD [32,34] extended by the CPMD/Gromos QM/MM interface [27] in conjunction with a consistent AB force field for the MM part [26]. The simulations were carried out in the Born-Oppenheimer propagation mode employing the Perdew-Becke-Ernzerhof (PBE) functional and a plane-wave basis set truncated at 70 Ry together with dual-space pseudopotentials for the QM part. Liquid AB comprises 343 *cis* AB molecules in a cubic 45.2 Å box subject to periodic boundary conditions. Therein a single AB molecule was treated quantum mechanically in an 18 Å cubic box using cluster boundary conditions [32]. Initial conditions for five na-QM/MM simulations were sampled from a standard QM/MM ground-state run at 400 K and extended, after vertical $S_0 \rightarrow S_1$ photoexcitation at $t=0$, to 500 fs in the nonadiabatic propagation mode. Five reference gas-phase nonadiabatic QM runs of a single AB molecule have been performed analogously using the same setup as for the QM part of the na-QM/MM calculations. ROKS agrees within ≈0.1 eV with the CASPT2 S_1 relative minimum energy profile [35] along the dihedral angle $\mathrm{C}^{(1)}\mathrm{NN}'\mathrm{C}^{(1')} \in [40,160]^\circ$ and reproduces CASSCF(14,12) data computed along a nonadiabatic dynamical path.

In order to allow for a full analysis of photoswitching, internal motion is described based on plane normal vectors $\mathbf{n}^{\mathrm{R}}$ and $\mathbf{n}^{\mathrm{R}'}$ of the two rings at their geometric centers, R and R′, together with such vectors $\mathbf{n}^{\mathrm{N}}$ and $\mathbf{n}^{\mathrm{N}'}$ of the $\mathrm{C}^{(1)}\mathrm{NN}'$ and $\mathrm{NN}'\mathrm{C}^{(1')}$ coordination planes at N and N′ (see Fig. 1). Next, order parameters $\varphi^{\alpha}(t) = \angle(\mathbf{n}^{\alpha}(t), \mathbf{n}^{\alpha}(0))$ are introduced to describe absolute motion in time relative to the $t=0$ configuration at vertical excitation, whereas $\varphi^{\alpha\beta}(t) = \angle(\mathbf{n}^{\alpha}(t), \mathbf{n}^{\beta}(t))$, $\alpha, \beta \in \{\mathrm{N}, \mathrm{N}', \mathrm{R}, \mathrm{R}'\}$ monitor relative changes as a function of time. In particular, φ^{R} and φ^{N} measure angular motion of the ring R and N coordination plane with respect to their orientation at photoexcitation, $\varphi^{\mathrm{NN}'}$ is the usual $\mathrm{C}^{(1)}\mathrm{NN}'\mathrm{C}^{(1')}$ dihedral angle, and φ^{RN} captures the rotation of the aromatic ring R relative to the N-coordination plane of the azo group. These generalized order parameters will prove crucial in unraveling new details of the photoisomerization mechanism.

A first impression of representative AB photoswitching is obtained from Fig. 2, which illustrates the torsional motion about the NN′ bond for *cis* to *trans* photoisomerization in the liquid phase and for an isolated molecule reference. As a result of the significantly different forces in the excited state, $\varphi^{\mathrm{NN}'}$ increases steeply in *both* cases from its small initial value in the *cis* ground state to reach ≈90° within only <50 fs after vertical $S_0 \rightarrow S_1$ excitation at $t=0$. This defines the first, ultrafast relaxation time scale. After a-nonadiabatic $S_1 \rightarrow S_0$ hop has occurred, typically around 200 fs, $\varphi^{\mathrm{NN}'}$ relaxes in another ≈50 fs thereafter to the *trans* equilibrium value of ≈180° in both cases, thus signaling a successful switching to *trans* AB; note that typically several repopulations of S_1 followed by decay back to S_0 occur.

In the gas phase, the dynamics of $\varphi^{\mathrm{NN}'}$ appears similar to what has been observed in semiempirical nonadiabatic dynamics [17,21]. Based on such standard analysis of only the dihedral angle $\varphi^{\mathrm{NN}'}$, the naive conclusions would be that (i) photoswitching follows the out-of-plane rotation pathway, and (ii) the same mechanism holds in both the liquid and gas phase. However, the situation is more intricate, as will be worked out in the following.

Taking a closer look at the motion of the N and N′ atoms and the geometric centers of the rings R and R′, as measured by their root-mean-square displacements (rmsd's) with respect to $t=0$ (see the insets of Fig. 2), reveals that N and N′ are moving most whereas the positions of the rings barely

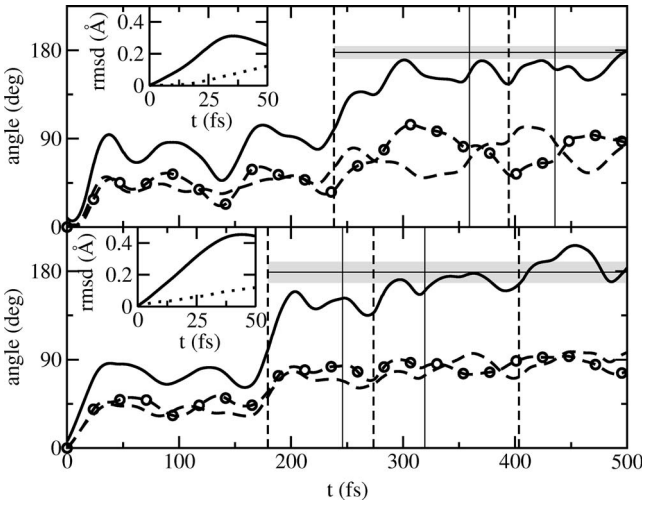

FIG. 2. *Cis-trans* photoswitching of AB in the liquid (top) and gas phase (bottom) based on typical na-QM/MM trajectories. Time evolution of $\varphi^{NN'}$ (—), φ^{N} (- -), and $\varphi^{N'}$ (○- -○) after vertical $S_0 \rightarrow S_1$ photoexcitation at $t=0$. Vertical dashed and solid lines indicate $S_1 \rightarrow S_0$ decay and $S_0 \rightarrow S_1$ reexcitation events. Shaded areas mark the fluctuation ranges about $\varphi^{NN'} \approx 180°$ from standard *trans* ground-state QM/MM simulations. Insets show the rmsd's of N,N′ (solid) and R,R′ (dashed) relative to $t=0$.

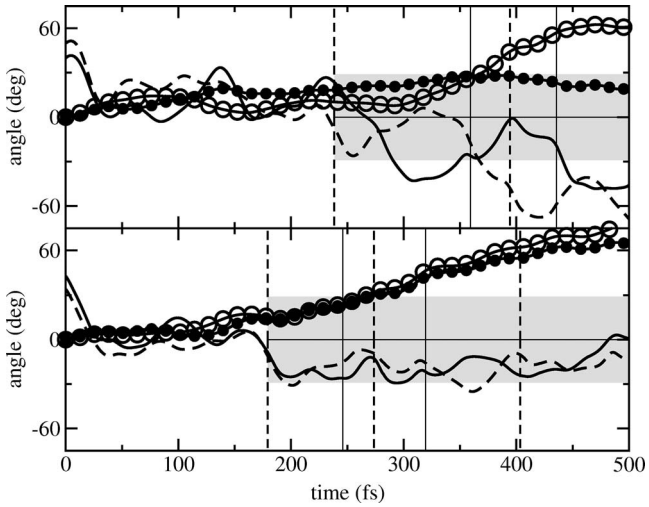

FIG. 3. Time evolution of φ^{RN} (--), $\varphi^{R'N'}$ (—), φ^{R} (○—○), and $\varphi^{R'}$ (●—●) in the liquid (top) and gas phase (bottom) with fluctuation ranges about $\varphi^{RN}/\varphi^{R'N'} \approx 0°$ shaded; see caption of Fig. 2.

change. This implies that the steep initial increase of $\varphi^{NN'}$ to 90° is *not* due to rotation of the aromatic rings, but results predominantly from the motions of N and N′ and, to a somewhat lesser extent, $C^{(1)}$ and $C^{(1')}$. Furthermore, monitoring the time evolution of φ^{N} and $\varphi^{N'}$ shows that $\varphi^{N}(t)+\varphi^{N'}(t) \approx \varphi^{NN'}(t)$ together with $\varphi^{N}(t) \approx \varphi^{N'}(t)$ holds up to the first $S_1 \rightarrow S_0$ decay in both the liquid and gas phase. This is another indicator that only motions of N and N′ together with $C^{(1)}$ and $C^{(1')}$ establish the total *cis* to *trans* switch detected by the $0° \rightarrow 180°$ increase of the dihedral angle $\varphi^{NN'}$.

Finally, φ^{RN} and $\varphi^{R'N'}$ (Fig. 3) steeply decrease in both setups from ≈50° to ≈0° within 50 fs, where they keep fluctuating in S_1. At the same time, φ^{R} and $\varphi^{R'}$, the orientations of both aromatic rings, remain essentially frozen at their $t=0$ values. In other words, this implies that the two coordination planes of N and N′ become coplanar with the adjacent aromatic rings. Again, this tells us that it must be the azo group, $C^{(1)}NN'C^{(1')}$, that *twists* in both cases relative to the two essentially space-fixed aromatic rings during S_1 dynamics instead of invoking a rotation of the rings. It is important to note that twisting and rotation pathways yield the same time evolution of the dihedral angle $\varphi^{NN'}$ and thus cannot be distinguished without additional order parameters such as those introduced here. Furthermore, the complex twisting mechanism uncovered precludes satisfactory classical modeling of photoswitching of AB functional units by simply adding an external mechanical potential acting exclusively on $\varphi^{NN'}$ forcing it to rotate from 0° to 180°, as done in earlier studies in the absence of appropriate simulation methods such as the one introduced here.

We have now firmly established that—in liquid and gas phase alike—the first stage (<50 fs) is dominated by a twisting motion, in which the N/N′ and $C^{(1)}/C^{(1')}$ atoms are displaced rather than the rings, in contrast to the "classic" *cis-trans* rotation with space-fixed N atoms and moving rings. Also throughout the second stage of S_1 dynamics between the first 50 fs and the first $S_1 \rightarrow S_0$ deexcitation, both systems are seen to behave similarly with $\varphi^{NN'}$ fluctuating around 90° (Fig. 2). Can we thus conclude that there is no difference between photoswitching in vacuum and in condensed matter? A first hint that this is not the case is provided by Fig. 2: concerted motion [i.e., $\varphi^{N}(t) \approx \varphi^{N'}(t)$] holds in the gas phase during the entire time evolution shown, whereas this is true in the liquid only during the first and second stages of excited-state evolution, i.e., up to about 200 fs. *Only after* relaxation to the S_0 state does the condensed phase environment break the symmetry of this concerted twisting, which leads to relative deviations as large as 40°–50° and heralds a third, slow relaxation stage beyond 200 fs.

Even more pronounced is the influence of the liquid state on the order parameters analyzed in Fig. 3. In vacuum, φ^{RN} and $\varphi^{R'N'}$ as well as φ^{R} and $\varphi^{R'}$ follow each other closely at all times, signaling synchronized aromatic ring rotation, whereas their motion becomes largely uncorrelated in the solvent after AB has relaxed back to S_0. Furthermore, φ^{RN} and $\varphi^{R'N'}$ reach their equilibrium range about 500 fs after photoexcitation only in the gas phase, whereas this relaxation process occurs on the picosecond time scale in the liquid. These effects can be traced back to steric confinement of typically one of the two bulky rings by neighbors in locally close-packed configurations. Again, *none* of these insights can be revealed by monitoring only the dihedral angle $\varphi^{NN'}$ as often done. In fact, it has been suggested [36] that a more complex "hula twist" model similar to the twisting motion unraveled in this work may indeed have to be considered to explain experimental findings. Our detailed mechanism explains convincingly why ultrafast, subpicosecond S_1 decay components measured experimentally do not vary strongly for "rotation-restricted" and "open" AB derivatives [36,37],

and why they show little solvent dependence [4]. On the other hand, pronounced effects of solvent viscosity and environmental confinement have been revealed for relaxation on the picosecond scale [4,36,37], in full agreement with our findings. This behavior has important ramifications on understanding and optimizing photoactive materials such as liquid crystals or thin films which exploit light-induced volume or shape changes [1,2].

In summary, a nonadiabatic QM/MM simulation method tailored for complex molecular condensed-matter systems has been developed and applied to compare photoswitching of AB in the liquid to the gas phase. In both cases, the pathway consists initially of a twisting of the central azo group while keeping the aromatic rings essentially frozen in space. In this initial two-stage process, the central CNNC dihedral angle changes first in the excited state from $\approx 0°$ (*cis*) to $\approx 90°$ in <50 fs, where it stays for ≈ 200 fs, before relaxing rapidly to $\approx 180°$ (*trans*) after a nonadiabatic transition to the ground state. Only thereafter does movement of the bulky rings finally set in. In vacuum, this molecular motion still follows molecular symmetry and leads to full relaxation in less than 1 ps. In the condensed phase, this third stage is heavily influenced by steric hindrance and local confinement leading to uncorrelated motion and relaxation times on the picosecond scale and beyond. The central CNNC torsion, which is often taken as the sole order parameter to analyze photoswitching, is insensitive to these phenomena. These insights not only explain experimental findings but also call into question modeling approaches where photoswitching is mimicked by mechanical rotation about the CNNC dihedral. The method introduced here is of a general nature and can be applied readily to a variety of photoactive condensed-matter systems such as liquid crystals, organic thin films, bulk polymers, or proteins.

We thank G. Mathias and N. Nair for technical help, C. Peter, L. Delle Site, and K. Kremer for discussions, VW Stiftung and FCI for funding, and NIC, SSCK, BOVILAB@RUB, and RV-NRW for computer time.

[1] *Molecular Switches*, edited by B. L. Feringa (Wiley-VCH, Weinheim, 2001).
[2] *Photoreactive Organic Thin Films*, edited by Z. Sekkat and W. Knoll (Academic, San Diego, 2002).
[3] A. Natansohn and P. Rochon, Chem. Rev. (Washington, D.C.) **102**, 4139 (2002).
[4] C. Renner and L. Moroder, ChemBioChem **7**, 869 (2006).
[5] Z. F. Liu, K. Hashimoto, and A. Fujishima, Nature **347**, 658 (1990).
[6] T. Ikeda and O. Tsutsumi, Science **268**, 1873 (1995).
[7] H. Finkelmann, E. Nishikawa, G. G. Pereira, and M. Warner, Phys. Rev. Lett. **87**, 015501 (2001).
[8] S. Spörlein *et al.*, Proc. Natl. Acad. Sci. U.S.A. **99**, 7998 (2002).
[9] Y. Yu, M. Nakano, and T. Ikeda, Nature **425**, 145 (2003).
[10] T. Hugel *et al.*, Science **296**, 1103 (2002).
[11] W. R. Browne and B. L. Feringa, Nat. Nanotechnol. **1**, 25 (2006).
[12] A. Khan, C. Kaiser, and S. Hecht, Angew. Chem., Int. Ed. **45**, 1878 (2006).
[13] J. Li, G. Speyer, and O. F. Sankey, Phys. Rev. Lett. **93**, 248302 (2004).
[14] M. Del Valle *et al.*, Nat. Nanotechnol. **2**, 176 (2007).
[15] T. Ishikawa, T. Noro, and T. Shoda, J. Chem. Phys. **115**, 7503 (2001).
[16] A. Cembra *et al.*, J. Am. Chem. Soc. **126**, 3234 (2004).
[17] A. Toniolo, C. Ciminelli, M. Persico, and T. Martinez, J. Chem. Phys. **123**, 234308 (2005).
[18] W.-G. Diau, J. Phys. Chem. A **108**, 950 (2004).
[19] M. L. Tiago, S. Ismail-Beigi, and S. G. Louie, J. Chem. Phys. **122**, 094311 (2005).
[20] C. R. Crecca and A. E. Roitberg, J. Phys. Chem. A **110**, 8188 (2006).
[21] G. Granucci and M. Persico, Theor. Chem. Acc. **117**, 1131 (2007), and references therein.
[22] P. Sherwood, in *Modern Methods and Algorithms of Quantum Chemistry*, edited by J. Grotendorst (NIC, Jülich, 2000).
[23] N. L. Doltsinis and D. Marx, Phys. Rev. Lett. **88**, 166402 (2002).
[24] N. L. Doltsinis and D. Marx, J. Theor. Comput. Chem. **1**, 319 (2002).
[25] J. C. Tully, J. Chem. Phys. **93**, 1061 (1990).
[26] M. Böckmann *et al.*, J. Chem. Theory Comput. **3**, 1789 (2007).
[27] A. Laio, J. VandeVondele, and U. Rothlisberger, J. Chem. Phys. **116**, 6941 (2002).
[28] I. Frank *et al.*, J. Chem. Phys. **108**, 4060 (1998).
[29] S. Grimm, C. Nonnenberg, and I. Frank, J. Chem. Phys. **119**, 11574 (2003); **119**, 11585 (2003).
[30] H. Langer, N. L. Doltsinis, and D. Marx, ChemPhysChem **6**, 1734 (2005).
[31] P. R. L. Markwick and N. L. Doltsinis, J. Chem. Phys. **126**, 175102 (2007).
[32] D. Marx and J. Hutter, in *Modern Methods and Algorithms of Quantum Chemistry*, edited by J. Grotendorst (NIC, Jülich, 2000), www.theochem.rub.de/go/cprev.html.
[33] S. R. Billeter and D. Egli, J. Chem. Phys. **125**, 224103 (2006).
[34] J. Hutter *et al.*, CPMD package; see www.cpmd.org.
[35] L. Gagliardi *et al.*, Theor. Chem. Acc. **111**, 363 (2004).
[36] T. Pancur *et al.*, Phys. Chem. Chem. Phys. **7**, 1 (2005).
[37] Y.-C. Lu, E. W.-G. Diau, and H. Rau, J. Phys. Chem. A **109**, 2090 (2005).